

Nature of Xenon adsorption on graphite: On-top versus hollow site preference

Juarez L. F. Da Silva^{1,*} and Catherine Stampff^{2,†}

¹*Institut für Chemie, Humboldt-Universität zu Berlin, Unter den Linden 6, D-10099 Berlin, Germany*

²*The School of Physics, The University of Sydney, Sydney, New South Wales 2006, Australia*

(Received 17 April 2007; revised manuscript received 25 May 2007; published 1 August 2007)

We study the interaction between Xe adatoms and the graphite (0001) surface employing all-electron density-functional theory calculations. Xe adatoms prefer to adsorb in the hollow site, which is consistent with a recent dynamical low-energy electron diffraction intensity analysis. We explain the hollow site preference as a consequence of the greater polarization of Xe adatoms at the hollow site, as well as of the surface C atoms, and hence a greater induced dipole moment, which provides a larger contribution to the attractive interaction. As a consequence, Xe adatoms get closer to the surface in the hollow site. The above-mentioned mechanisms of the interaction between Xe atoms and graphite (0001) are, thus, very similar to the picture recently proposed for rare-gas adatoms on close-packed metal surfaces.

DOI: [10.1103/PhysRevB.76.085301](https://doi.org/10.1103/PhysRevB.76.085301)

PACS number(s): 68.43.-h, 68.43.Bc, 68.43.Fg

I. INTRODUCTION

Rare-gas (RG) atom adsorption on solid surfaces may be regarded as the paradigm of a simple physical adsorption system, in which it is typically assumed that the weak interaction is determined by an interplay of van der Waals attraction and Pauli repulsion.^{1,2} In early studies, this interaction was often described by empirical pair potentials such as Lennard-Jones (LJ),¹ which favors close-packed RG solid structures³ and hollow sites of RG adatoms on graphite⁴ and metal surfaces.⁵ These trends led to the expectation that RG adatoms preferentially bind to high coordination sites on solid surfaces in general.¹

In contrast, quantitative low-energy electron diffraction (LEED) intensity analysis^{6–11} and density-functional theory (DFT) calculations^{12–18} have found that RG adatoms preferentially bind at the on-top sites on close-packed transition-metal surfaces such as Ti(0001), Cu(111), Pd(111), and Pt(111), more as a rule and not as an exception. DFT calculations^{15–18} attributed the on-top adsorption site preference to be a consequence of the site-dependent Pauli repulsion and polarization of the RG adatoms and topmost substrate atoms. The Pauli repulsion is weaker at the on-top site due to the “donorlike” behavior of the metal d_{z^2} states, which allow the RG adatoms to get closer to the metal surface. A polarization of the RG adatoms by the metal surface gives rise to an induced dipole moment pointing out of the surface, which results in a decrease of the substrate work function in accord with experimental results.

Recent dynamical LEED studies¹⁹ and DFT calculations,²⁰ employing the pseudopotential plane-wave (PPPW) method, found that Xe adatoms preferentially bind at the hollow sites on graphite (0001) in the $(\sqrt{3} \times \sqrt{3})R30^\circ$ structure (from now on labeled $\sqrt{3}$), which is in agreement with the “old” picture based on two-pair LJ potential results; i.e., Xe adatoms bind to highly coordinated adsorption sites. The mechanism, however, for the Xe hollow site preference on graphite (0001) was not addressed in Refs. 19 and 20. It was suggested in Ref. 20 that the attractive interaction between the Xe atoms and the graphite (0001) surface results from the hybridization of the C $2p$ states with the Xe $5p$ and

$6s$ states, i.e., very much as in a chemisorbed system.

Therefore, the interaction mechanism proposed for Xe adatoms on graphite (0001) differs from the interaction mechanism reported for RG adatoms on transition-metal surfaces.^{15–18} Hence, it is not clear if the picture proposed for the interaction between RG atoms and transition-metal surfaces can be extended to different solid surfaces. To investigate this, we perform all-electron full-potential L/APW+lo calculations for Xe adatoms on graphite (0001) in the $\sqrt{3}$ structure. Our calculations confirm the Xe hollow site preference on graphite (0001). An analysis of the work function change, electron density differences, reactivity function, atomic geometry, and density of states shows that the RG-metal model interaction based on calculations for RG-(close-packed) metal systems can be applied to describe the interaction between Xe atoms and the graphite (0001) surface and can explain the Xe hollow site preference.

II. THEORETICAL AND COMPUTATIONAL DETAILS

Our calculations are performed using DFT^{21,22} with the local density approximation²³ (LDA) for the exchange-correlation functional. The Kohn-Sham equations are solved using the all-electron full-potential L/APW+lo method,^{24–26} as implemented in the WIEN2K code,^{26–28} which is a combination of the linearized augmented plane-wave (LAPW) method²⁴ and of the augmented plane wave plus local orbitals (APW+lo) method.²⁵ The electronic states are described at the scalar-relativistic approximation; i.e., the core states are treated fully relativistically by taking into account the spin-orbit coupling, while it is neglected for the semicore and valence states.

Inside the atomic spheres with radii of 0.64 and 1.27 Å for C and Xe, respectively, APW+lo basis functions are used for $l=0, 1, 2$, while LAPW basis functions are used for $l=3, 4, \dots, 12$. Furthermore, local orbitals are set to specifically treat the Xe $5d$ semicore states. The L/APW+lo wave functions in the interstitial region are represented using plane waves with kinetic energies up to 25 Ry. For the potential representation in the interstitial region, plane waves with kinetic energies up to 256 Ry are considered, while inside the

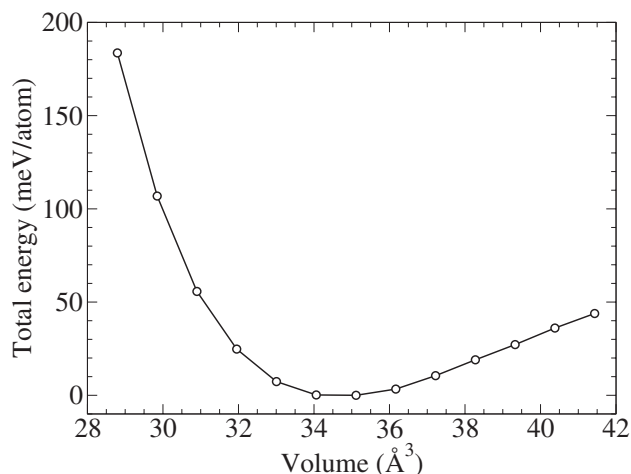


FIG. 1. Total energy per atom of bulk graphite as a function of the volume. The total energy is given with respect to the total energy calculated at the equilibrium volume.

atomic spheres, angular momenta up to 6 are taken into account. Nonspherical matrix Hamiltonian elements are considered up to $l=6$.

The clean graphite (0001) surface and Xe/graphite (0001) systems are modeled by six C layers in the slab separated by a vacuum region of 19.70 Å employing (1×1) and $\sqrt{3}$ surface unit cells, respectively. The Xe atoms are adsorbed on both sides of the slab. The Brillouin zone (BZ) integrations are performed using a Monkhorst-Pack²⁹ (MP) grid with a broadening of the Fermi surface by the Fermi distribution function with an artificial broadening parameter of 27 meV. The total energy is extrapolated to $T=0$ K.³⁰ Only inversion and identity symmetries are employed for the Xe/graphite calculations. Hence, exactly the same \mathbf{k} point set is used for all Xe/graphite calculations. We employ MP grids of $(10 \times 10 \times 3)$, $(10 \times 10 \times 1)$, and $(4 \times 4 \times 1)$ for the bulk, the clean graphite (0001) surface, and the Xe/graphite (0001), respectively, which correspond to 28, 14, and 8 \mathbf{k} points in the irreducible part of the BZ. For density of states calculations, a MP grid twice as dense is employed, i.e., $(8 \times 8 \times 1)$ for Xe/graphite (0001) calculations.

III. RESULTS

A. Bulk and clean surface properties of graphite

To determine the equilibrium volume of bulk graphite with *ABAB* stacking, we perform calculations for 13 regularly spaced volumes in which the c/a ratio is optimized for each volume. The equilibrium volume ($V_0 = \sqrt{3}a_0^2c_0/2$) is obtained by fitting the relaxed potential energy by a polynomial function (see Fig. 1). The spin-polarized total energy of the free C atom, which is required to evaluate the cohesive energy E_{coh} is calculated using a cubic box with a side length of 10.58 Å and one \mathbf{k} point, $(\frac{1}{4}, \frac{1}{4}, \frac{1}{4})\frac{2\pi}{a}$,³¹ in the irreducible part of the BZ. The results are obtained at 0 K, and no corrections are made for the zero point energy. The bulk properties are summarized in Table I.

TABLE I. Bulk properties of graphite with *ABAB* stacking. Equilibrium lattice constants (a_0, c_0) and cohesive energy per atom, E_{coh} .

Method		a_0 (Å)	c_0 (Å)	E_{coh} (eV)
L/APW+lo ^a	LDA	2.45	6.57	-8.93
USPP ^b	LDA	2.44	6.64	-8.90
Expt.		2.46 ^c	6.67 ^c	-7.37 ^d
Expt.			6.71 ^e	

^aPresent work.

^bReference 34.

^cReference 32; 0 K.

^dBrewer, as cited in Ref. 33.

^eReference 32; ≈ 300 K.

The LDA equilibrium lattice constants, a_0 and c_0 , are in good agreement with experimental results;³² e.g., a_0 and c_0 deviate by -0.41% and -2.09% , respectively. Furthermore, our LDA results are in good agreement with similar LDA calculations summarized in Ref. 34. However, the same level of agreement is not found for the cohesive energy, in which the LDA overestimates E_{coh} by almost 21% compared with experiment,³³ on the other hand, it has been reported that LDA underestimates the binding energy between the graphite layers.³⁴ We note that various available generalized gradient approximations for the exchange-correlation energy functional give no binding, or bind very weakly, layered structures such as graphite,^{34,35} as well as the adsorption of rare-gas adatoms on metal surfaces.¹⁵⁻¹⁸

The valence band maximum (VBM) and the conduction band minimum (CBM) are located at the special \mathbf{k} point K , which are degenerate in energy and have a p_z symmetry. Similar results have been obtained by previous LDA calculations,³⁶ while experimentally, an overlap of the VBM and CBM of ≈ 0.04 eV has been reported.³⁷ The LDA bandwidth ($K-\Gamma$) is 19.56 eV, while the experimental result is 22.0 eV;³⁸ i.e., LDA underestimates the bandwidth by almost 11%. This deviation is reduced to $\approx 1\%$ by performing quasiparticle calculations.³⁸ The local density of states show that the electronic states from -3.0 eV to slightly above the Fermi level have a p_z symmetry, i.e., perpendicular to the graphite planes, while the electronic states at a lower energy have a p_{x+y} symmetry.

Calculations for the clean graphite (0001) surface are carried out, employing slabs with four, six, and eight layers. We found negligible changes in the vertical interlayer spacings; i.e., there is almost no relaxation of the graphite (0001) surface. As mentioned above, we chose to use six layers in our adsorption studies. We found a work function Φ of 4.492 eV for the graphite (0001) surface, which is in reasonable agreement with the experimental value of 4.7 eV,³⁹ with a deviation of only 0.21 eV (4.4%), which is similar to the deviations reported for transition-metal surfaces.⁴⁰

B. Xe adsorption on graphite

Calculations are performed for Xe adatoms on graphite (0001) in the $\sqrt{3}$ structure, in which there is one Xe adatom

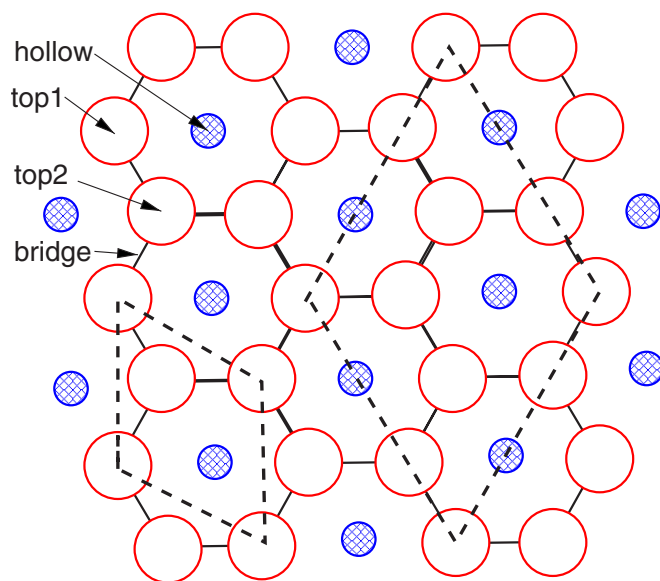


FIG. 2. (Color online) Schematic top view of the graphite (0001) surface. The large open circles (red) indicate the C atoms in the topmost surface layer, while the small hatched (blue) circles indicate the C atoms in the second plane. The (1×1) and $(\sqrt{3} \times \sqrt{3})R30^\circ$ surface unit cells are indicated to the left and right of the picture, respectively. The high-symmetry adsorption sites are also indicated. There are two types of top sites, top1 and top2, which differ by one (top1) having a second-layer C atom directly below it, while the other (top2) does not.

per six C atoms in the topmost surface layer (see Fig. 2). In contrast to the close-packed metal fcc(111) surfaces, in which the Xe adatom at the hollow site is threefold coordinated, on the graphite (0001) surface, the Xe adatoms at the hollow sites are sixfold coordinated. Furthermore, the area of the hollow site in the graphite (0001) surface (hexagonal area) is smaller than the area of the hollow site in the fcc(111) surface (triangle area), e.g., 5.21 \AA^2 for graphite (0001) and 6.41 \AA^2 for Xe/Pd(111). Four adsorption sites are considered, namely, the hollow, bridge, and two top sites, which are six-, two-, and onefold coordinated, respectively. There are two types of top sites (top1 and top2), which differ by one (top1) having a second-layer C atom directly below it, while the other top site (top2) does not.

Due to the weak interaction between Xe adatoms and graphite (0001), as well as to the absence surface relaxations, the C atoms of the substrate are kept fixed in their unrelaxed

TABLE II. Adsorption properties of Xe on graphite (0001) in the $\sqrt{3}$ structure. Equilibrium vertical distance $d_{\text{Xe-graphite}}$, relative total energies with respect to the hollow site, $\Delta E = E_{\text{tot}}^{\text{site}} - E_{\text{tot}}^{\text{hollow}}$, and work function change $\Delta\Phi = \Phi^{\text{Xe-graphite}} - \Phi^{\text{graphite}}$.

Adsorption sites	$d_{\text{Xe-graphite}}$ (Å)	ΔE (meV)	$\Delta\Phi$ (meV)
Hollow	3.497	0.00	103
Bridge	3.581	5.51	84
Top1	3.584	6.24	83
Top2	3.583	6.33	87

atomic positions. The positions of the Xe adatoms are fully optimized. The equilibrium vertical distances, $d_{\text{Xe-graphite}}$, relative total energies, and work function changes are summarized in Table II.

Our calculations show that the Xe adatoms preferentially adsorb in the highly coordinated hollow sites, which is lower in energy by almost 6 meV than the top sites. Both top sites (top1 and top2) are degenerate in energy, while the bridge site is just ≈ 0.7 meV more favorable than the top sites. The hollow site preference is consistent with a recent dynamical LEED study performed for Xe on graphite (0001).¹⁹ Furthermore, it is in agreement with previous PPPW calculations employing the LDA functional,²⁰ which obtained an energy difference of 4.9 meV between the hollow and top sites. The hollow site preference has also been obtained by PPPW calculations for Kr and Ar adatoms on graphite (0001).^{41,42}

The relative energy difference between the hollow and top sites (6 meV) is in excellent agreement with the corrugation potential of Xe adatoms on graphite (0001) obtained by the analysis of experimental measurements [3.29,⁴³ 6.64,⁴⁴ and 6.47 meV (Ref. 45)]. Furthermore, due to the small corrugation potential energy, the commensurate-incommensurate structural transition might occur even at low temperatures.⁴³

We find an equilibrium distance of Xe to the surface of 3.497 \AA , which is in very good agreement with the value of $3.59 \pm 0.04 \text{ \AA}$ obtained by the LEED study¹⁹ and with the PPPW calculations (3.60 \AA).²⁰ Furthermore, our results indicate that the Xe adatoms get slightly closer to the surface in the hollow sites than in the top sites, i.e., $d_{\text{Xe-graphite}}^{\text{hollow}} < d_{\text{Xe-graphite}}^{\text{top}}$, which is intuitively expected according to results based on Lennard-Jones type potentials.^{3,4} We note that in Ref. 20, in which one graphite sheet was used to represent the surface, the distance of Xe from the surface was reported to be the same (3.60 \AA) for all three sites considered (hollow, top, and bridge). The hollow site preference and the smaller equilibrium vertical distance obtained for Xe on graphite (0001) in the hollow site found in the present work are in contrast to the trends found by DFT studies for Xe adsorption on metal surfaces.¹⁵⁻¹⁸ These studies reported that Xe adatoms adsorb preferentially in the top sites and get closer to the surface at the top sites compared to the hollow site.

The interaction energy between the Xe layer and the graphite surface is calculated by the following equation: $\frac{1}{2}(E_{\text{tot}}^{\text{Xe-graphite}} - E_{\text{tot}}^{\text{graphite}} - 2E_{\text{tot}}^{\text{Xe layer}})$, where $E_{\text{tot}}^{\text{Xe-graphite}}$ is the total energy of the Xe-graphite system at the equilibrium configuration. $E_{\text{tot}}^{\text{graphite}}$ and $E_{\text{tot}}^{\text{Xe layer}}$ are the total energies of graphite (0001) and a freestanding Xe layer, respectively. The Xe layer is calculated with the same lateral lattice as that used for the Xe-graphite calculations. We obtained an interaction energy of -168 meV, while previous PPPW calculations reported -204 meV.²⁰ The total energies given, with respect to the hollow site, are summarized in Table II. In Refs. 41 and 42, the adsorption energies from PPPW calculations reported for Kr and Ne on graphite (0001) are 106 and 86 meV, respectively, and the corresponding vertical distances above the hollow site are 3.35 and 3.20 \AA . This trend of a decreasing height with decreasing size of the RG atom can be understood largely on the basis of a hard sphere picture: Using the experimental lattice constant of graphite,

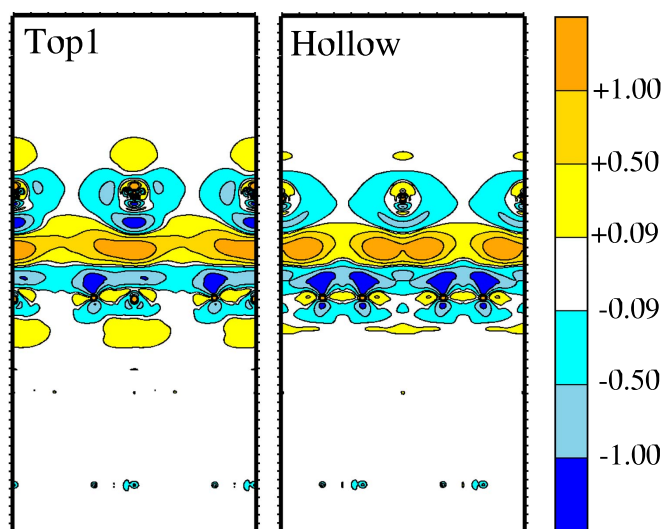


FIG. 3. (Color online) Difference electron density $n^{\Delta}(\mathbf{r})$ plots for the equilibrium configuration of Xe on graphite (0001). $n^{\Delta}(\mathbf{r})$ is given in $10^{-3}e/\text{bohr}^3$. Yellow, gold, and orange (cyan, sky-blue, and blue) indicate regions where the electron density increases (decreases).

together with the van der Waals radii of Xe, Kr, and Ne (of 2.16, 2.02, and 1.88 Å) and the van der Waals radius of C (of 1.7 Å) for the RG-graphite interaction, vertical heights of 3.59, 3.44, and 3.29 Å are predicted, in close correspondence to the calculated values.

In Table II, we list the work function change $\Delta\Phi$ of the graphite (0001) surface due to the adsorption of Xe atoms. $\Delta\Phi = \Phi^{\text{Xe-graphite}} - \Phi^{\text{graphite}}$, where $\Phi^{\text{Xe-graphite}}$ and Φ^{graphite} are the work functions of the Xe-graphite system and the clean surface, respectively. We find $\Phi^{\text{graphite}} = 4.492$ eV and $\Phi^{\text{Xe-graphite}} = 4.595$ eV (hollow); hence, $\Delta\Phi = 103$ meV (hollow), which is in excellent agreement with the experimental result of ≈ 100 meV.⁴⁶ For Xe adatoms in the bridge and in both top1 and top2 sites, $\Delta\Phi \approx 83$ meV. This result is opposite to the trend obtained for Xe/metal surfaces, in which the work function of the metal surface decreases upon Xe adsorption by almost ≈ 1.0 eV for systems such as Xe/Pt(111) in the $\sqrt{3}$ structure.¹⁵⁻¹⁷

To obtain a better understanding of the results mentioned above, as well as of the interaction between Xe atoms and graphite (0001), we calculate the difference electron density plots, $n^{\Delta}(\mathbf{r})$, which help to characterize the atomic orbitals involved in the interaction between the adsorbate and the substrate. $n^{\Delta}(\mathbf{r}) = n^{\text{Xe-graphite}}(\mathbf{r}) - n^{\text{graphite}}(\mathbf{r}) - n^{\text{Xe layer}}(\mathbf{r})$, where $n^{\text{Xe-graphite}}(\mathbf{r})$ is the electron density of Xe on graphite (0001). $n^{\text{graphite}}(\mathbf{r})$ and $n^{\text{Xe layer}}(\mathbf{r})$ are the electron density of the clean surface and the Xe adlayer, respectively. The plots in a plane perpendicular to the surface, and passing through the Xe atoms, are shown in Fig. 3.

The difference electron density distributions show a significant decrease in electron density about the Xe atoms and a delocalized enhancement below them. For the top site, an enhancement of electron density can also be noticed toward the top of the Xe atoms. A depopulation of the C $2p$ states perpendicular to the surface ($2p_z$ states) and a (slight) popu-

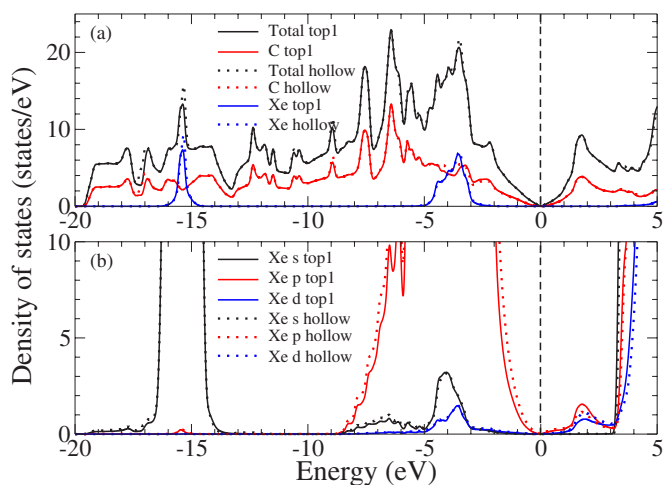


FIG. 4. (Color online) Total and local density of states (DOS) calculated at the equilibrium Xe-graphite geometry for Xe in the on-top (top1) and hollow sites. (a) Total and local (C and Xe) DOSs; (b) decomposition of the Xe local DOS in their s , p , and d contributions. The Xe local DOSs are multiplied by 10^3 in (b). The vertical dashed lines indicate the Fermi level.

lation of the C $2p$ states parallel to the surface, i.e., $2p_x$ and $2p_y$ states, can also be seen. This trend is stronger for Xe adatoms in the hollow site, while there is almost no depopulation of the C $2p_z$ states for the C atoms located directly below the Xe adatom for the top site. For Xe adatoms in the top sites, the electron density redistribution is stronger on the C atoms *not* located directly below the Xe adatoms. Thus, $n^{\Delta}(\mathbf{r})$ indicates that the polarization of the substrate (C atoms) is very efficient for the configuration in which Xe adatoms are located in the hollow sites.

The complex redistribution of electron density gives rise to a net surface dipole moment that points inward toward the surface and a slight work function increase. Due to the small magnitude of the work function change, i.e., ≈ 100 meV, this is not immediately obvious from the difference electron density plots in Fig. 3. The larger electron density redistribution for Xe adatoms in the hollow site, however, is consistent with the larger work function change for Xe adatoms in the hollow site.

The picture described above is supported by the “Wilke function” analysis,⁴⁷ which characterizes the reactivity of solid surfaces based on the study of changes in the electronic states close to the Fermi level due to the broadening of the occupation numbers in the Fermi distribution. It is useful in the study of reactions where the interactions between the reactants are weak, which is the case for Xe adatoms on graphite (0001). The Wilke function analysis indicates that the C p_z states perpendicular to the surface are most easily depopulated, which is expected since these states dominate the density of states close to the Fermi level. Furthermore, this analysis does not indicate an increase of electron density in the hollow site region, which is also consistent with the difference electron density analysis. Such an increase of electron density would generate an increased Pauli repulsion between the Xe atom and the adsorption site.

We now consider the density of states (DOS). The total and local DOSs are calculated at the equilibrium geometry

employing an $(8 \times 8 \times 1)$ \mathbf{k} point mesh. The results for Xe adatoms in the on-top (top1) and hollow sites are plotted in Fig. 4. As obtained for the graphite bulk and surface (0001), there is no band gap between the highest occupied and lowest unoccupied states. The local DOS shows that the Xe states are shifted several electron volts below the Fermi level, i.e., the center of gravity of the Xe $5p$ and $5s$ states are 3.8 and 15.3 eV below the Fermi level, respectively. For Xe adatoms in the on-top and hollow sites, we find a slight depopulation of the Xe $5p$ states and population of the previously unoccupied Xe states with an sd character, which follows a similar trend as for Xe adatoms on metal surfaces.¹⁶ However, in contrast to the adsorption of Xe atoms on metal surfaces such as Pd(111), we cannot identify significant differences between the local DOS for Xe adatoms in the on-top and hollow sites for the Xe-graphite system. Such *almost* identical Xe local DOSs for both adsorption sites on graphite are a consequence of the small energy difference (≈ 6 meV) between the sites.

We explain the hollow site preference for Xe adatoms on graphite (0001) based on the following observations: (i) The polarization is larger for Xe in the hollow site; i.e., the induced dipole moment is greater. Thus, it contributes a greater attractive interaction between the Xe atoms and the graphite surface, which is also supported by the shortest equilibrium vertical distance. (ii) The electron density difference and Wilke function analysis indicates no electron density accumulation in the hollow site region, hence, suggesting that the Pauli repulsion is weaker at the hollow site, which allows the Xe adatoms to get closer to the surface, enhancing the hollow site preference.

Moreover, LEED intensity analysis and DFT calculations find that Xe adatoms preferentially bind in the on-top and hollow sites on close-packed metal and graphite (0001) surfaces, respectively, and suggest that the interaction mechanism for both cases are very similar.¹⁵⁻¹⁸ For both systems, the polarization of the adsorbate and the substrate (topmost surface layer) and the site-dependent Pauli repulsion determine the Xe adsorption site preference. Which site that is depends on the nature of the substrate.

IV. SUMMARY

In the present work, we performed all-electron DFT-LDA calculations for the adsorption of Xe atoms on the graphite (0001) surface in the $\sqrt{3}$ structure. We found that Xe adatoms preferentially adsorb in the hollow site, which is consistent with a LEED intensity analysis.¹⁹ We explain the hollow site preference as a consequence of the larger polarization of Xe adatoms in the hollow site and of the surface C atoms (larger induced dipole moment) and a weaker Pauli repulsion. This provides a larger contribution to the attractive interaction, and the Xe adatoms get closer to the surface. For all sites, we find a slight depopulation of the Xe $5p$ states and population of the previously unoccupied Xe states with an sd character. Thus, very similar trends observed for Xe adatoms on close-packed metal surfaces¹⁵⁻¹⁸ are obtained for Xe adatoms on graphite (0001).

ACKNOWLEDGMENT

We thank the Australian Center for Advanced Computing and Communication for computer time.

*Present address: National Renewable Energy Laboratory, 1617 Cole Blvd., Golden, Colorado 80401, USA; juarez_dasilva@nrel.gov

†Electronic address: stampfl@physics.usyd.edu.au

¹L. W. Bruch, M. W. Cole, and E. Zaremba, *Physical Adsorption: Forces and Phenomena* (Oxford Science, Oxford, 1997).

²G. Vidali, G. Ihm, H.-Y. Kim, and M. W. Cole, *Surf. Sci. Rep.* **12**, 133 (1991).

³N. W. Ashcroft and N. M. Mermin, *Solid State Physics* (Holt-Saunders International Editions, 1976).

⁴W. E. Carlos and M. W. Cole, *Surf. Sci.* **91**, 339 (1980).

⁵J. R. Cerdá, P. L. de Andres, F. Flores, and R. Perez, *Phys. Rev. B* **45**, 8721 (1992).

⁶B. Narloch and D. Menzel, *Chem. Phys. Lett.* **290**, 163 (1997).

⁷Th. Seyller, M. Caragiu, R. D. Diehl, P. Kaukasoina, and M. Lindroos, *Chem. Phys. Lett.* **291**, 567 (1998).

⁸Th. Seyller, M. Caragiu, and R. D. Diehl, *Surf. Sci.* **454**, 55 (2000).

⁹M. Caragiu, G. S. Letherman, Th. Seyller, and R. D. Diehl, *Surf. Sci.* **475**, 89 (2001).

¹⁰M. Caragiu, Th. Seyller, and R. D. Diehl, *Phys. Rev. B* **66**, 195411 (2002).

¹¹M. Caragiu, Th. Seyller, and R. D. Diehl, *Surf. Sci.* **539**, 165 (2003).

¹²J. E. Müller, *Phys. Rev. Lett.* **65**, 3021 (2001).

¹³A. E. Betancourt and D. M. Bird, *J. Phys.: Condens. Matter* **12**, 7077 (2000).

¹⁴S. Clarke, G. Bihlmayer, and S. Blügel, *Phys. Rev. B* **63**, 085416 (2001).

¹⁵J. L. F. Da Silva, Ph.D. thesis, Technical University of Berlin, Berlin, Germany, 2002 (http://edocs.tu-berlin.de/diss/2002/dasilva_juarez.htm or <http://www.fhi-berlin.mpg.de/th/pub02.html>).

¹⁶J. L. F. Da Silva, C. Stampfl, and M. Scheffler, *Phys. Rev. Lett.* **90**, 066104 (2003).

¹⁷J. L. F. Da Silva, C. Stampfl, and M. Scheffler, *Phys. Rev. B* **72**, 075424 (2005).

¹⁸J. L. F. Da Silva and C. Stampfl, *Phys. Rev. B* (to be published).

¹⁹K. Pussi, J. Smerdon, N. Ferralis, M. Lindroos, R. MacGrath, and R. D. Diehl, *Surf. Sci.* **548**, 157 (2004).

²⁰X.-R. Chen, X.-L. Zhou, J. Zhu, and Q.-Q. Gou, *Phys. Lett. A* **315**, 403 (2003).

²¹P. Hohenberg and W. Kohn, *Phys. Rev.* **136**, B864 (1964).

²²W. Kohn and L. J. Sham, *Phys. Rev.* **140**, A1133 (1965).

²³J. P. Perdew and Y. Wang, *Phys. Rev. B* **45**, 13244 (1992).

²⁴D. J. Singh, *Plane Waves, Pseudopotentials and the LAPW Method* (Kluwer Academic, Boston, 1994).

²⁵E. Sjöstedt, L. Nordstöm, and D. J. Singh, *Solid State Commun.*

- 114**, 15 (2000).
- ²⁶G. K. H. Madsen, P. Blaha, K. Schwarz, E. Sjöstedt, and L. Nordström, *Phys. Rev. B* **64**, 195134 (2001).
- ²⁷P. Blaha, K. Schwarz, P. Sorantin, and S. B. Trickey, *Comput. Phys. Commun.* **59**, 399 (1990).
- ²⁸K. Schwarz, P. Blaha, and G. K. H. Madsen, *Comput. Phys. Commun.* **147**, 71 (2002).
- ²⁹H. J. Monkhorst and J. D. Pack, *Phys. Rev. B* **13**, 5188 (1976).
- ³⁰M. G. Gillan, *J. Phys.: Condens. Matter* **1**, 689 (1989).
- ³¹M. Fuchs, J. L. F. Da Silva, C. Stampfl, J. Neugebauer, and M. Scheffler, *Phys. Rev. B* **65**, 245212 (2002).
- ³²Y. Baskin and L. Meyer, *Phys. Rev.* **100**, 544 (1955).
- ³³M. T. Yin and M. L. Cohen, *Phys. Rev. B* **29**, 6996 (1984).
- ³⁴M. Hasegawa and K. Nishidate, *Phys. Rev. B* **70**, 205431 (2004).
- ³⁵H. Rydberg, M. Dion, N. Jacobson, E. Schröder, P. Hyldgaard, S. I. Simak, D. C. Langreth, and B. I. Lundqvist, *Phys. Rev. Lett.* **91**, 126402 (2003).
- ³⁶N. A. W. Holzwarth, S. G. Louie, and S. Rabii, *Phys. Rev. B* **26**, 5382 (1982).
- ³⁷M. S. Dresselhaus, G. Dresselhaus, and P. C. Eklund, *Science of Fullerenes and Carbon Nanotubes* (Academic, San Diego, 1996), p. 17.
- ³⁸C. Heske, R. Treusch, F. J. Himpsel, S. Kakar, L. J. Terminello, H. J. Weyer, and E. L. Shirley, *Phys. Rev. B* **59**, 4680 (1999).
- ³⁹A. R. Law, J. J. Barry, and H. P. Hughes, *Phys. Rev. B* **28**, 5332 (1983).
- ⁴⁰J. L. F. Da Silva, C. Stampfl, and M. Scheffler, *Surf. Sci.* **600**, 703 (2006).
- ⁴¹X.-R. Chen, A. Oshiyama, and S. Okada, *Chem. Phys. Lett.* **371**, 528 (2003).
- ⁴²X.-R. Chen, A. Oshiyama, and S. Okada, *Phys. Rev. B* **67**, 033408 (2003).
- ⁴³H. Hong, C. J. Peters, A. Mak, R. J. Birgeneau, P. M. Horn, and H. Suematsu, *Phys. Rev. B* **40**, 4797 (1989).
- ⁴⁴G. Vidali and M. W. Cole, *Phys. Rev. B* **29**, 6736 (1984).
- ⁴⁵T. Halpin-Healy and M. Kardar, *Phys. Rev. B* **34**, 6557 (1986).
- ⁴⁶T. Mandel, M. Domke, G. Kaindl, C. Laubschat, M. Prietsch, U. Middlemann, and K. Korn, *Surf. Sci.* **162**, 453 (1985).
- ⁴⁷S. Wilke, M. H. Cohen, and M. Scheffler, *Phys. Rev. Lett.* **77**, 1560 (1996).